JACS
JOURNAL OF THE AMERICAN CHEMICAL SOCIETY
Communication
pubs.acs.org/JACS

Melting Proteins: Evidence for Multiple Stable Structures upon Thermal Denaturation of Native Ubiquitin from Ion Mobility Spectrometry-Mass Spectrometry Measurements

Tarick J. El-Baba,[†] Daniel W. Woodall,[†] Shannon A. Raab,[†] Daniel R. Fuller,[†] Arthur Laganowsky,[‡] David H. Russell,[‡] and David E. Clemmer*[,†]

[†]Department of Chemistry, Indiana University, 800 Kirkwood Avenue, Bloomington, Indiana 47401, United States
[‡]Department of Chemistry, Texas A&M University, College Station, Texas 77843, United States

Supporting Information

ABSTRACT: Ion mobility and mass spectrometry techniques are coupled with a temperature-controlled electrospray ionization source to follow the structural transitions of ubiquitin in aqueous solution (pH = 3) at elevated solution temperatures (T = 26−96 °C). Changes in the charge state distribution are consistent with a two-state, cooperative unfolding transition having a melting temperature of T_m = 71 ± 2 °C, in agreement with prior measurements [Wintrode, P. L.; Makhatadze, G. I.; Privalov, P. L. *Proteins*, **1994**, *18*, 246−253]. However, analysis of ion mobility distributions reveals the two-state transition is a composite of transitions involving at least nine unique species: three native or native-like structures; two that appear to be equilibrium intermediates (i.e., populations of new conformers that form at elevated temperatures but subsequently disappear at higher temperatures); and four products observed at high temperatures, including the well-characterized ubiquitin A state, and two solution species that are differentiated based on a *cis*- or *trans*-configured Glu[18]-Pro[19] peptide bond. These nine states vary in abundances by factors as large as ∼10^3 over the range of solution temperatures. Although experimental melting transitions are conceived as a loss of well-defined structure leading to a random distribution of unstructured, denatured forms, the results provide evidence for new conformers having at least some well-defined structural elements are stabilized as temperature is increased.

A temperature-controlled electrospray ionization (ESI) emitter, coupled to a hybrid ion mobility spectrometry-mass spectrometry (IMS-MS) instrument, is used to investigate ubiquitin structures over a range of solution temperatures. At low temperatures, IMS-MS distributions reflect populations of native ubiquitin in solution. As temperature is increased, changes in mobility and charge state distributions reveal emergence of multiple solution species, as the folded state becomes thermally unstable and disappears. It appears the evaporative-cooling phenomenon associated with droplet shrinkage[1−23] during the ESI process[4] "freezes out"[5,6] the populations of at least nine different solution conformers favored at different solution temperatures. Once dehydrated, different ion conformations can be delineated based on differences in mobilities and charge states.[7−9] The ability to follow populations of structures in solution by monitoring gaseous ions complements traditional solution techniques and provides insight about structure and stability.

Protein structures can be altered by many types of perturbations, including introduction of chaotropes,[10] variation of pH,[11] and thermal heating.[12] Although melting of a protein is conceived as a cooperative two-state process, involving the loss of the well-defined folded structure of the native state to form a distribution of random, amorphous forms,[12] it is postulated that different types of intermediate structures should be populated near the melting temperature, T_m.[13] However, the cooperative nature of the transition, coupled with the transient nature of intermediates, inhibits direct experimental observation of such species. The results below provide evidence for many well-defined structures stabilized during a melting transition.

Nested IMS-MS measurements were carried out using a home-built 3 m-drift tube/time-of-flight instrument described elsewhere.[14] Aqueous solutions of ubiquitin (15 μM, pH 3) were pumped through a temperature-controlled capillary and ESI emitter[15] assembly such that solutions incubate at a defined temperature (±1 °C) for ∼10 min prior to analysis (see Supporting Information). The inset in Figure 1 shows mass spectra obtained upon analysis of solutions incubated and electrosprayed at three different temperatures: 26, 70, and 96 °C. At 26 °C, $[M+7H]^{7+}$ dominates the mass spectrum.

As the temperature is increased, higher charge states centered around the $[M+11H]^{11+}$ species are favored. This shift in charge state signifies a structural change and is interpreted as evidence for a folded to denatured transition.[16−18] A plot of the weighted charge state intensities at each temperature[19] gives rise to the sigmoidal curve shown in Figure 1. This curve resembles a typical cooperative two-state melting transition;[12,20,21] the midpoint yields the experimental melting temperature, T_m = 71 ± 2 °C, in agreement with T_m = 73 °C (at pH = 3) from microcalorimetry measurements[22] as well as other reports.[23]

Insight about the species involved in melting can be gleaned from ion mobility measurements. An ion's mobility through a buffer gas is related to its shape.[24−26] Thus, extended conformers have larger collision cross sections and lower mobilities than

Received: March 20, 2017
Published: April 20, 2017

DOI: 10.1021/jacs.7b02774
J. Am. Chem. Soc. 2017, 139, 6306−6309

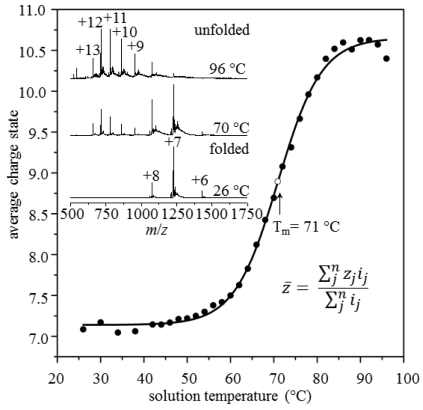

Figure 1. Weighted average charge state as function of solution temperature having a midpoint at $T_m = 71 \pm 2$ °C. Inset shows selected mass spectra that undergo a global charge state shift as a solution temperature is increased.

smaller, more compact, folded structures.[7−9,27,28] Because the only experimental variable we change in these studies is solution temperature, ion mobility distributions provide a readout on thermally induced structural changes as well as the relative abundance of each species.

Figure 2 shows at 26 °C the ion-mobility cross section distributions for $[M+6H]^{6+}$and $[M+7H]^{7+}$ (i.e., major signals at low temperatures) are centered at 970 and 1007 Å^2, respectively, indicating these ions have compact structures. There is also a compact form of $[M+8H]^{8+}$, the sharp peak at 1010 Å^2; this peak comprises ∼5% of this distribution, which is dominated by broader features at higher cross sections, as discussed below. The experimental cross sections for these compact ions are somewhat smaller than the calculated trajectory value[29] for the atomic coordinates of the crystal structure (Ω_{calc} = 1090 Å^2);[30,31] molecular dynamics (MD) simulations yield structures having $\Omega(MD)_{calc}$ = 1030 ± 20 Å^2, consistent with experiment (see Supporting Information). When solvent is removed from the native structure, the anhydrous gas-phase ion contracts slightly, as external side chains and exposed backbone regions interact with one another to maximize internal charge solvation, hydrogen bonds, and van der Waals interactions.[8,32] However, the general β-grasp fold of the native state,[33] in which the Ile^{23}-Glu^{34} helical region interacts with the five stranded β-sheet (formed upon hydrogen-bonding of the distant Met^1-Lys^6 and Glu^{64}-Arg^{72} regions), appears to be preserved in the gas phase.[30,31] As the temperature is raised, abundances of the compact $[M+6H]^{6+}$ and $[M+7H]^{7+}$ species decrease, as higher charge state ions emerge from solution. Total abundance of $[M+8H]^{8+}$ remains relatively unchanged (from 26 to ∼80 °C); instead, this species appears sensitive to a conformational shift that increases intensities of the broad features from ∼1100 to 1550 Å^2.

Close inspection of the $[M+8H]^{8+}$ cross section distributions reveals two small sharp peaks at Ω = 1635 and 1650 Å^2, favored at high temperatures. These peaks are a signature of ions that represent the ubiquitin A state.[31] Figure 2 illustrates the solution structure of the A state, derived from NMR studies;[34] this is the most abundant form of ubiquitin in aqueous solutions containing ∼30−70% methanol,[31,34] having substantially more helical content than the native state. The A state retains the native N-terminal Met^1-Val^{17} β-sheet. However, the β-sheet associated with the native Gln^{40}-Arg^{72} residues transforms into an elongated α-helix. Although abundance of the A state in the present studies is small (<1% of the total population), it is accessible and stable even at our highest solution temperatures. Its observation demonstrates thermal denaturation of the native fold can produce highly structured products.

It is interesting to examine the loss of the native state with increasing temperature in more detail. Consider the abundance profiles of $[M+6H]^{6+}$and $[M+7H]^{7+}$ species shown in Figure 2. Each plot is effectively an independent melting curve. The $[M+7H]^{7+}$ species, comprising ∼70% of the ions produced from low-temperature solutions, begins to decrease in abundance at ∼60 °C and by ∼80 °C this species is substantially depleated. Analysis of this smooth sigmoidal melting curve yields $T_m = 71 \pm 2$ °C, the expected melting temperature. The $[M+6H]^{6+}$ species is less abundant, comprising only ∼10% of the total population at 26 °C. The melting curve for $[M+6H]^{6+}$ shows this species decays earlier and more gradually, having an experimental T_m = 60 ± 1 °C. The different shapes and melting temperatures for the $[M+6H]^{6+}$ and $[M+7H]^{7+}$ species require the presence of unique species in solution, presumably two native-like structures (designated as N_2 and N_1, respectively) having slightly different stabilities. A similar analysis for the sharp, low-abundance Ω($[M+8H]^{8+}$ = 1010 Å^2) peak, which also disappears with increasing temperature, shows this species persists to ∼70 °C and thus is more stable than the $[M+6H]^{6+}$ and $[M+7H]^{7+}$ conformers. Analysis of the melting curve for this structure yields $T_m = 74 \pm 2$ °C. This is evidence for a third native-like structure (N_3) of different abundance and stability.

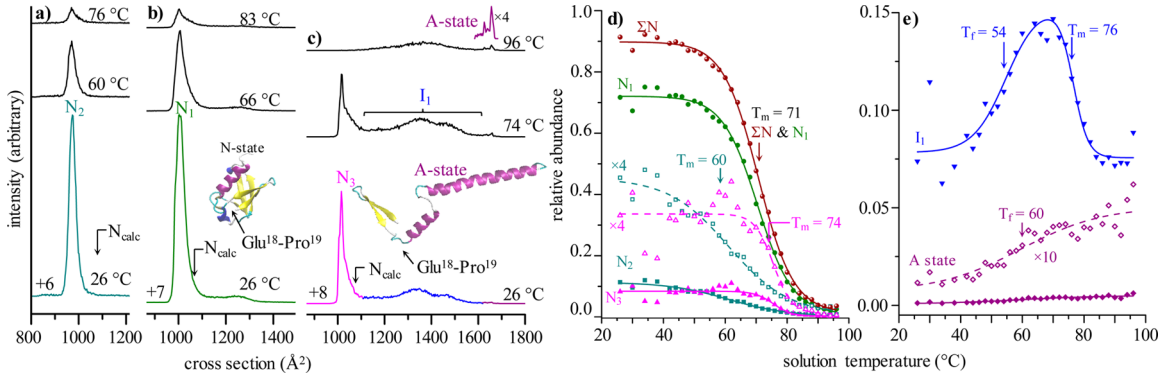

Figure 2. Cross section distributions for (a) $[M+6H]^{6+}$, (b) $[M+7H]^{7+}$, and (c) $[M+8H]^{8+}$ ions of ubiquitin at various temperatures. Also shown are abundance profiles for (d) native conformations (N_1, N_2, N_3) and their sum ($\sum$N), and (e) growth and decay of the intermediate state (I_1) and emergence of the A state as product of melting. The position of Glu^{18}-Pro^{19} is indicated in each structure.

DOI: 10.1021/jacs.7b02774
J. Am. Chem. Soc. 2017, 139, 6306−6309

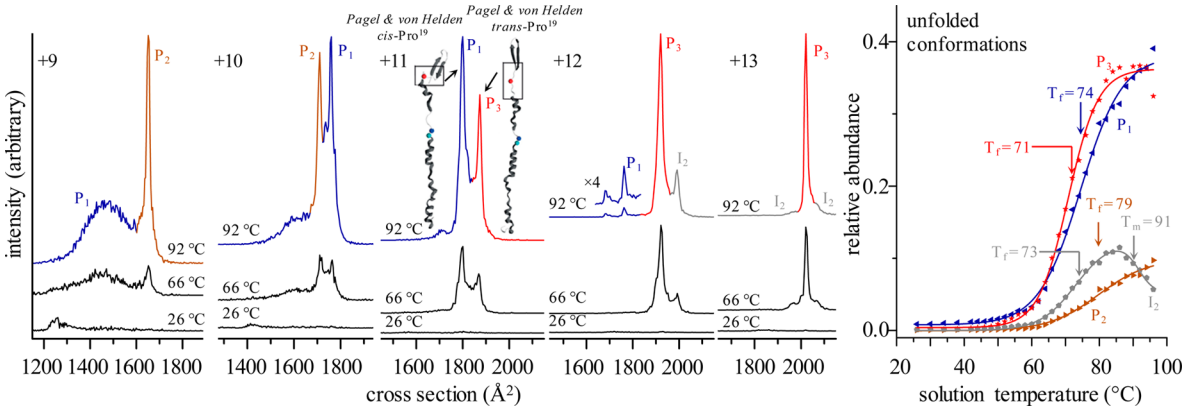

Figure 3. Collision cross section distributions for $[M+9H]^{9+}$ – $[M+13H]^{13+}$ ions of ubiquitin at various temperatures. Traces are shown in different colors when IMS peaks for different charge states show indistinguishable temperature profiles (see below and Supporting Information). The last panel shows abundance profiles as a function of temperature for each configuration, revealing three distinct solution products (P_1, P_2, and P_3) and one high-temperature equilibrium intermediate (I_2). Structures are adapted from ref 35.

As a cross check, analysis of the sum of all three mobility-based melting curves, i.e., weighted average of the three discrete populations shown in Figure 2, yields T_m = 71 ± 2 °C, in agreement with the expected melting temperature. The ability to discern coexisting species (even those low in abundance) by IMS-MS makes this method sensitive to subtle differences missed upon analysis of the ensemble average. This provides a new way of interpreting a protein denaturation transition.

This analysis can be extended to other parts of the IMS-MS data sets. Integrations of each of the broad peaks between Ω ~1100 and 1550 Å^2 for $[M+8H]^{8+}$ (Figure 2) shows no significant variation in the melting temperatures or profiles for any of these features. Although this could be interpreted as evidence for multiple solution species showing identical melting behavior, it is also consistent with a single type of solution species that upon ionization forms multiple gas phase structures. The latter explanation is simplest. Thus, we assign cross sections from 1100 to 1550 Å^2 to a single type of solution species and assume upon dehydration it evolves to form many different anhydrous structures. Interestingly, the abundance profile for this region appears to rise and then fall with increasing temperature. Analysis yields a formation temperature (T_f) of 54 ± 2 °C. These species reach a maximum population of ~15% at a solution temperature of ~60 °C. Beyond this temperature, the population decreases, with T_m = 76 ± 1 °C. Stability over such a narrow range suggests this species arises from a delicate balance of forces. That this population appears as a product of relatively low-temperature melting and then undergoes a subsequent structural transition, causing it to disappear at higher temperatures, requires it must contain some structure, or it would not melt. Thus, we consider it an equilibrium intermediate and designate it the I_1 solution structure. The relatively low formation temperature suggests it may arise, at least in part, from the least stable N_2 native-like structure upon melting.

Figure 3 shows results obtained upon analyzing the $[M+9H]^{9+}$ to $[M+13H]^{13+}$ species, favored at high temperatures. These are products of melting. In many cases, regions of the ion mobility distributions for these charge states yield melting curves indistinguishable from one another based on their shapes as well as T_m values. For example, the abundance curves from integration of the sharp peaks for $[M+9H]^{9+}$ and $[M+10H]^{10+}$ species centered at Ω = 1650 and 1710 Å^2, respectively (shown in brown), have different intensities but nearly identical shapes, independently yielding values of T_m = 79 ± 1 and 79 ± 1 °C for these respective species (see Supporting Information). Because of this similarity, as well as the similar cross sections and mobility peak shapes, we assume the same type of solution species yields these two experimental peaks. This population is a stable product (designated as P_2) arising from the loss of other species favored at lower temperatures. P_2 persists to our highest solution temperature (96 °C).

A similar analysis suggests other features in high charge states emerge from a minimum of three additional types of solution products, formed from melting other states (see Supporting Information). One of these products begins to disappear beyond ~85 °C, with a subsequent T_m = 91 ± 1. This solution population appears to also be an equilibrium intermediate (I_2), stabilizing some structural element upon formation at intermediate temperatures that becomes unstable at higher temperatures. The other two products, P_1 and P_3, formed at high temperatures, yield T_f = 74 ± 2 and 71 ± 2 °C, respectively, and also persist to the highest temperature. The P_1 curve is the sum of intensities from peaks within $[M+9H]^{9+}$, $[M+10H]^{10+}$, and $[M+11H]^{11+}$ having Ω = 1500, 1760, and 1800 Å^2, respectively, as well as the two tiny $[M+12H]^{12+}$ peaks at Ω = 1680 and 1760 Å^2. Recently, Pagel, von Helden, and co-workers used an elegant ultraviolet photodissociation approach to demonstrate the Ω($[M+11H]^{11+}$ = 1800 Å^2) peak corresponds to a conformer in which the Glu^{18}-Pro^{19} peptide bond exists in a *cis* configuration.[35] In this geometry, interactions with nearby residues protect the Glu^{18}-Pro^{19} bond from fragmentation. Because of the identical cross sections measured here, we speculatively assign the P_1 species as the Pagel and von Helden *cis*-structure, and P_3 as the corresponding *trans*-structure. The *trans*-configured Glu^{18}-Pro^{19} peptide bond is succeptable to fragmentation because it lacks local stabilizing interactions. Visual inspection of the solution-formation curves for these species (Figure 3) shows the *trans*-structure is favored (from ~80 to 90 °C). Presumably, solution interactions, or interactions with distal regions of the peptide chain accessible in the *trans*-configuration, stabilize this species. We note a *trans*-configured Glu^{18}-Pro^{19} bond is a key element of the native structure, acting as a hinge allowing intimate interactions between the N-terminal Met^1-Lys^6 and C-terminal Glu^{64}-Arg^{72} residues that establish the parallel *β*-sheet. We anticipate the less thermally stable *cis*-configured P_3 species lacks these distant interactions.

Figure 4 shows relative abundances of solution structures as a function of temperature. Over the 3 orders of magnitude shown,

DOI: 10.1021/jacs.7b02774
J. Am. Chem. Soc. 2017, 139, 6306–6309

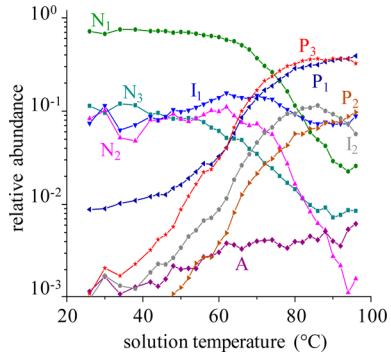

Figure 4. Relative abundances as a function of solution temperature for all nine conformations.

nearly every species is present across the temperature range. This plot illustrates the complexity associated with a thermally induced transition involving many states. As a final experiment, we tested the reversibility of this system by incubating our ubiquitin solution at 90 °C prior to cooling and analysis at 26 °C. The results (see Supporting Information) are indistinguishable from data obtained without high-temperature incubation, indicating this system is reversible. The ability to discern many distinct solution populations and structures by IMS-MS provides a glimpse into species stabilized at different temperatures and provides insight on how the energy landscape changes with temperature. Such studies will be complemented by advances in ensemble and single-molecule techniques, (e.g., relaxation-dispersion nuclear magnetic resonance[36] and single-molecule force spectroscopy,[37] respectively) that revealed sparsely populated transient states previously undetected.

■ ASSOCIATED CONTENT

Supporting Information

The Supporting Information is available free of charge on the ACS Publications website at DOI: 10.1021/jacs.7b02774.

Experimental details (PDF)

■ AUTHOR INFORMATION

Corresponding Author

*clemmer@indiana.edu

ORCID

David E. Clemmer: 0000-0003-4039-1360

Notes

The authors declare no competing financial interest.

■ ACKNOWLEDGMENTS

This work is supported in part by funds from the Waters Corporation, the National Institutes of Health, R01 GM103725-02 (D.C.), as well as R21NS094882 (A.L.) and DP2GM123486 (A.L.), and the U.S. Department of energy, DE-FG02-04ER15520, (D.R.).

■ REFERENCES

(1) Lee, S.-W.; Freivogel, P.; Schindler, T.; Beauchamp, J. *J. Am. Chem. Soc.* **1998**, *120*, 11758−11765.

(2) McAllister, R. G.; Metwally, H.; Sun, Y.; Konermann, L. *J. Am. Chem. Soc.* **2015**, *137*, 12667−12676.

(3) Kim, D.; Wagner, N.; Wooding, K.; Clemmer, D. E.; Russell, D. H. *J. Am. Chem. Soc.* **2017**, *139*, 2981−2988.

(4) Fenn, J. B.; Mann, M.; Meng, C. K.; Wong, S. F.; Whitehouse, C. M. *Science* **1989**, *246*, 64−71.

(5) Pierson, N. A.; Chen, L.; Valentine, S. J.; Russell, D. H.; Clemmer, D. E. *J. Am. Chem. Soc.* **2011**, *133*, 13810−13813.

(6) Silveira, J. A.; Fort, K. L.; Kim, D.; Servage, K. A.; Pierson, N. A.; Clemmer, D. E.; Russell, D. H. *J. Am. Chem. Soc.* **2013**, *135*, 19147−19153.

(7) Clemmer, D. E.; Jarrold, M. F. *J. Mass Spectrom.* **1997**, *32*, 577−592.

(8) Jarrold, M. F. *Acc. Chem. Res.* **1999**, *32*, 360−367.

(9) Wyttenbach, T.; Pierson, N. A.; Clemmer, D. E.; Bowers, M. T. *Annu. Rev. Phys. Chem.* **2014**, *65*, 175−196.

(10) Myers, J. K.; Pace, N.; Scholtz, J. M. *Protein Sci.* **1995**, *4*, 2138−2148.

(11) Anderson, D. E.; Becktel, W. J.; Dahlquist, F. W. *Biochemistry* **1990**, *29*, 2403−2408.

(12) Jackson, S. E.; Fersht, A. R. *Biochemistry* **1991**, *30*, 10428−10435.

(13) (a) Brockwell, D. J.; Radford, S. E. *Curr. Opin. Struct. Biol.* **2007**, *17*, 30−37. (b) Daggett, V.; Fersht, A. R. *Nat. Rev. Mol. Cell Biol.* **2003**, *4*, 497−502. (c) Baldwin, R. L. *Annu. Rev. Biophys.* **2008**, *37*, 1−21.

(14) (a) Merenbloom, S. I.; Koeniger, S. L.; Valentine, S. J.; Plasencia, M. D.; Clemmer, D. E. *Anal. Chem.* **2006**, *78*, 2802−2809. (b) Koeniger, S. L.; Merenbloom, S. I.; Valentine, S. J.; Jarrold, M. F.; Udseth, H.; Smith, R. D.; Clemmer, D. E. *Anal. Chem.* **2006**, *78*, 4161−4174.

(15) See Supporting Information references 1−3 for similar designs.

(16) Chowdhury, S. L.; Katta, V.; Chait, B. T. *J. Am. Chem. Soc.* **1990**, *112*, 9012−9013.

(17) Loo, J. A.; Loo, R. R. O.; Udseth, H. R.; Edmonds, C. G.; Smith, R. D. *Rapid Commun. Mass Spectrom.* **1991**, *5*, 101−105.

(18) Mirza, U. A.; Cohen, S. L.; Chait, B. T. *Anal. Chem.* **1993**, *65*, 1−6.

(19) Benesch, J. L. P.; Sobott, F.; Robinson, C. V. *Anal. Chem.* **2003**, *75*, 2208−2214.

(20) Privalov, P. L. *Adv. Protein Chem.* **1979**, *33*, 167−241.

(21) Prabhu, N. V.; Sharp, K. A. *Annu. Rev. Phys. Chem.* **2005**, *56*, 521−548.

(22) Wintrode, P. L.; Makhatadze, G. I.; Privalov, P. L. *Proteins: Struct., Funct., Genet.* **1994**, *18*, 246−253.

(23) Cary, P. D.; King, D. S.; Crane-Robinson, C.; Bradbury, W. M.; Rabbani, A.; Goodwin, G. H.; Johns, E. W. *Eur. J. Biochem.* **1980**, *112*, 577−580.

(24) (a) Revercomb, H. E.; Mason, E. A. *Anal. Chem.* **1975**, *47*, 970−983. (b) Mason, E. A.; McDaniel, E. W. *Transport Properties of Ions in Gases*; Wiley: New York, NY, 1988.

(25) von Helden, G.; Hsu, M. T.; Kemper, P. R.; Bowers, M. T. *J. Chem. Phys.* **1991**, *95*, 3835−3837.

(26) Jarrold, M. F.; Constant, V. A. *Phys. Rev. Lett.* **1991**, *67*, 2994−2997.

(27) Clemmer, D. E.; Hudgins, R. R.; Jarrold, M. F. *J. Am. Chem. Soc.* **1995**, *117*, 10141−10142.

(28) Gidden, J.; Bushnell, J. E.; Bowers, M. T. *J. Am. Chem. Soc.* **2001**, *123*, 5610−5611.

(29) Mesleh, M. F.; Hunter, J. M.; Shvartsburg, A. A.; Schatz, G. C.; Jarrold, M. F. *J. Phys. Chem.* **1996**, *100*, 16082−16086.

(30) Wyttenbach, T.; Bowers, M. T. *J. Phys. Chem. B* **2011**, *115*, 12266−12275.

(31) Shi, H.; Pierson, N. A.; Valentine, S. J.; Clemmer, D. E. *J. Phys. Chem. B* **2012**, *116*, 3344−3352.

(32) Counterman, A. E.; Clemmer, D. E. *J. Am. Chem. Soc.* **1999**, *121*, 4031−4039.

(33) Vijay-Kumar, S.; Bugg, C. E.; Cook, W. J. *J. Mol. Biol.* **1987**, *194*, 531−544.

(34) (a) Harding, M. M.; Williams, D. H.; Woolfson, D. N. *Biochemistry* **1991**, *30*, 3120−3128. (b) Brutscher, B.; Brüschweiler, R.; Ernst, R. R. *Biochemistry* **1997**, *36*, 13043−13053. (c) Stockman, B. J.; Euvrard, A.; Scahill, T. A. *J. Biomol. NMR* **1993**, *3*, 285−296. (d) Cordier, F.; Grzesiek, S. *Biochemistry* **2004**, *43*, 11295−11301.

(35) Warnke, S.; Baldauf, C.; Bowers, M. T.; Pagel, K.; von Helden, G. *J. Am. Chem. Soc.* **2014**, *136*, 10308−10314.

(36) Sekhar, A.; Kay, L. E. *Proc. Natl. Acad. Sci. U. S. A.* **2013**, *110*, 12867−12874.

(37) Yu, H.; Siewny, M. G. W.; Edwards, D. T.; Sanders, A. W.; Perkins, T. T. *Science* **2017**, *355*, 945−950.

DOI: 10.1021/jacs.7b02774
J. Am. Chem. Soc. 2017, 139, 6306−6309